P-wave neutron strength-function measurements and the low-energy optical potential

H. S. Camarda*
National Bureau of Standards, Washington, D. C., 20234
(Received 2 August 1973)

Using the National Bureau of Standards electron linac and underground time-of-flight facility, precise average neutron-transmission measurements have been made in the energy range 1 keV $\leq E \leq$ 600 keV on the elements As, Br, Nb, Rh, Ag, In, Sb, I, La, Ho, Au, and Th. The samples were "thick" in that the s-wave self-protection had to be accounted for at low energies. However, the samples were still sufficiently thin that any errors introduced by neglecting p-wave self-protection were negligible. The average R-matrix theory was employed in the analysis and the $l=0$ scattering length R' and the p-wave strength function S_1 were extracted from the data. The behavior of S_1 vs mass number A in the region of the $3P$ maximum was found to vary smoothly with no evidence of any splitting of the resonance. Using Moldauer's optical potential, which fits the $l=0$ data well, the behavior of S_1 vs A was calculated. The predicted behavior was found to differ significantly from experiment. In particular, experiment indicates S_1 peaks at a lower mass number and that the maximum is stronger than indicated by the calculations. When the constants of the potential were changed in order to reproduce the observed behavior of S_1, a significant discrepancy with the $l=0$ data resulted. The results presented here imply an orbital angular momentum dependence of the low-energy optical potential.

[NUCLEAR REACTIONS As, Br, Nb, Rh, Ag, In, Sb, I, La, Ho, Au, Th; measured average neutron transmission $E=1-600$ keV; deduced R', p-wave strength function; optical-model analysis.]

INTRODUCTION

The study of the interaction of low-energy neutrons (E less than several MeV) with nuclei has had an important impact on the picture of how nucleons interact with the nucleus. Prior to the early 1950's it was believed that a low-energy neutron, upon entering the nucleus, promptly shared its energy with the nucleons of the nucleus. This view was motivated in part by the compound nuclear resonances induced by neutrons at eV energies. One of the implications of this strong absorption or black nucleus picture was that the *average* total cross section should vary smoothly with energy and mass number A.[1] Contrary to these predictions, average neutron cross-section measurements by Barschall *et al.*[2] demonstrated that maxima and minima vs E and A were prominent features. This indicated that the neutron does not immediately share its energy (and form a compound nucleus) upon entering the nucleus. These results and the fresh success of the nuclear shell model led Feshbach, Porter, and Weisskopf[3] to formulate the low-energy optical model for the neutron-nucleus interaction. The cross sections predicted by this model were, in the low-energy limit, to be compared with an average cross section which contained many fine-structure compound nuclear resonances. The only predicted cross section which is directly comparable with experiment is σ_T, the total cross section. Further, the shape elastic cross section σ_{SE} and the cross section for the compound-nucleus formation, σ_C, can also be calculated. Since σ_C includes elastic scattering via compound-nucleus formation, the measured elastic and reaction cross sections cannot be associated with σ_{SE} and σ_C. At higher energies where the compound nucleus can decay into many channels, σ_{SE} and σ_C can be associated with the measured elastic and reaction cross sections.

For neutrons of keV and lower incident energy $l=0$ interactions dominate. Many high-resolution experiments in the $\leq$10-keV energy range have determined the s-wave strength function $S_0=\langle\Gamma_n^0\rangle/\langle D\rangle$ and the $l=0$ elastic scattering length R' for a wide range of nuclei throughout the Periodic Table. $\langle\Gamma_n^0\rangle$ represents the average reduced neutron width of the $l=0$ levels and $\langle D\rangle$ their average spacing. In the keV region the total cross section exhibits the sharp structure of the compound nuclear resonances. An average of a sum of single level Breit-Wigner expressions yields:

$$\sigma_T^{l=0}=4\pi(R')^2+2\pi^2\lambda\!\!\!^{-2}(E/1\text{ eV})^{1/2}S_0. \tag{1}$$

The term $4\pi(R')^2$ is associated with the $l=0$ shape elastic cross section σ_{SE} of the optical model, while the second term, which is proportional to S_0, is associated with the compound-nucleus formation cross section σ_C. The low-energy optical model of Feshbach, Porter, and Weisskopf is found to be consistent with this data. For example, the observed maxima of S_0 at $A \sim 60$, 160 and minima of S_0 at $A \sim 100$, 230 are reproduced by the model.

Any optical potential determined by fits to R' and S_0 is representative of how an $l = 0$ neutron "sees" the nucleus. If the $l = 1$ interaction could be cleanly "measured" it would be interesting to discover whether the optical potential as determined by the s-wave data could describe, with equivalent accuracy, the p-wave data. A significant discrepancy might be indicative of an l dependence of the low-energy optical potential. This provides the main impetus for the experiment performed here.

At low energies[4] the p-wave interaction is usually expressed in terms of the p-wave strength function[5] $S_1 = \frac{1}{3}\langle g\Gamma_n^1\rangle / \langle D\rangle$, where $\langle g\Gamma_n^1\rangle$ is the average reduced neutron width times a spin factor g for the $l = 1$ levels and $\langle D\rangle$ their average spacing. The optical model predicts a maximum for S_1 around $A = 100$. Previous measurements of the p-wave strength function do show a peaking of S_1 near $A = 100$. However, the measurements are not sufficiently precise for a meaningful picture of the behavior of S_1 vs mass number to emerge. The methods usually employed to determine S_1 are:
(1) identification of $l = 1$ levels in a high-resolution experiment,
(2) average neutron-capture measurements,
(3) average total neutron cross section or transmission measurements.

The first method requires the necessary resolution, sample thickness, etc. to observe many of the small p levels. A knowledge of the smallest observable width vs energy is necessary, as is a method of distinguishing the p levels from the small s levels. A method of distinguishing p and s levels based on the known statistical behavior of neutron resonances has been described,[6] and a careful recent application of this approach is discussed in detail by Liou *et al.*[7]

The second method involves measuring the average neutron-capture cross section as a function of neutron energy, e.g., $0 \leq E \leq 200$ keV. The s-wave contribution is determined through a fitting procedure or by using $l = 0$ parameters determined in other experiments. The remaining capture cross section is assumed to be p wave, and S_1 is found by a best fit to the data. This approach is difficult experimentally, and further, the analysis usually assumes the s- and p-radiation widths are equal. Recent experimental data[8] indicate this can be a serious source of error. Pioneering neutron-capture measurements by Gibbons *et al.*[9] implied extremely large S_1 values in the $A = 100$ region. A more current measurement[10] using the same technique resulted again in much larger S_1 values in the region $A = 100$ than is reasonable.

The last approach is essentially an average total-cross-section measurement. As such it does not require a knowledge of neutron flux, detector efficiency, etc. The main disadvantage of this method is that below several hundred keV the $l = 0$ shape elastic cross section forms the major contribution to the average transmission. Consequently, very precise measurements are required for S_1 to be determined with good accuracy. Experiments of this nature performed on a few elements with the Harwell linac[11] are of good quality, and the values of S_1 determined here are in general agreement with their results. Other average transmission measurements performed at Brookhaven[12] (these experiments were not sufficiently precise and covered a significantly smaller energy range) and Duke[13] resulted in S_1 values which are in qualitative, but not quantitative, agreement with the results here. However, a current reanalysis of the Duke data[14] has lead to S_1 values in better agreement with those obtained here.

EXPERIMENT

Average transmission measurements were performed over the energy range 1 kev $\leq E \leq 600$ keV for a number of elements concentrating in the region $A = 100$. The measurements were carried out using the National Bureau of Standards electron linac as a pulsed source of neutrons in conjunction with an underground time-of-flight (TOF) facility. This TOF facility has been developed by Schwartz and his co-workers (see Ref. 15) for neutron cross-section measurements in the energy range 1 keV $\leq E \leq 1$ MeV.

The experimental setup for the transmission measurements performed here is depicted in Fig. 1. 80-MeV electrons strike a thick tungsten target producing neutrons which are moderated by an H_2O plus fluoroboric acid (HBF_4) mixture. The addition of fluoroboric acid to the water moderator resulted in a decrease in the observed background. This was due to the capture of slow neutrons by ^{10}B rather than hydrogen which produces a 2.2-MeV γ ray which is difficult to shield against. The relevant features of this moderator have been described in some detail elsewhere.[16] The 36-m flight path is shielded from the tungsten target and views only the moderator. A piece of bismuth was kept permanently in the neutron beam; this serves a twofold purpose. It reduces the γ flash

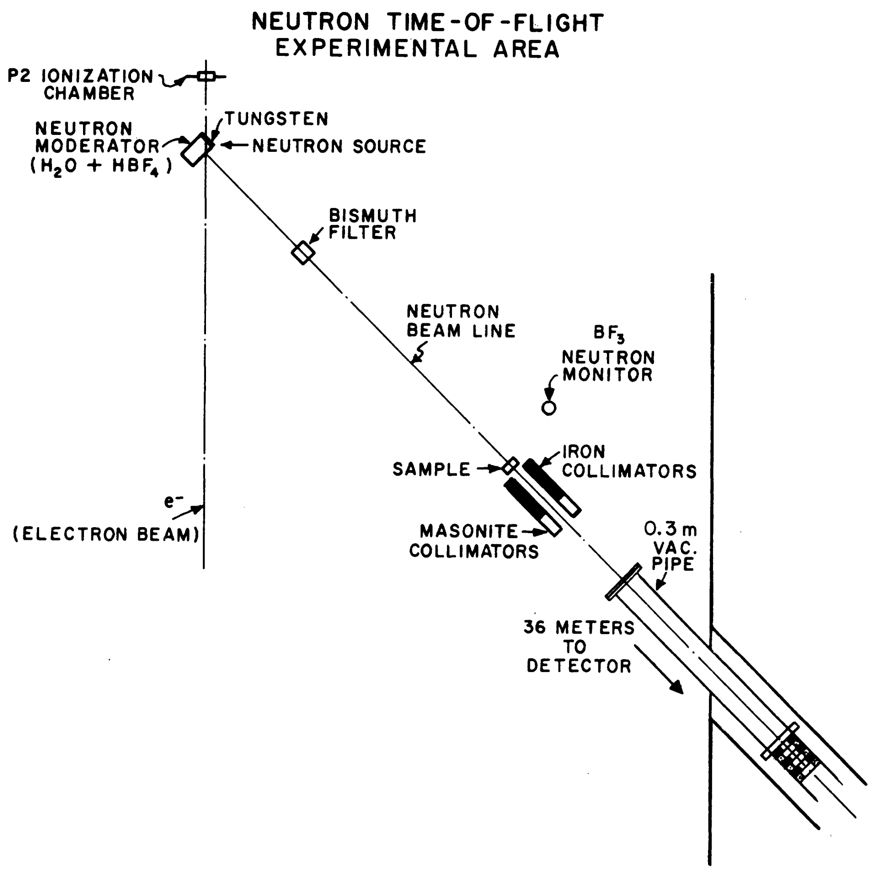

FIG. 1. Schematic view of the TOF experimental setup. 80-MeV electrons strike a thick tungsten target producing neutrons which are moderated by an H_2O plus fluoroboric acid (HBF_4) mixture. A bismuth filter 2.5 cm thick was permanently in the beam and samples of interest were cycled in and out of the beam every 10 min. The normalization of sample and open runs was provided for by the $P2$-ionization chamber and shielded BE_3 proportional counter. At 36 m 4 NaI detectors viewed 1 kg of ^{10}B housed in a 12.7-cm-diam container.

accompanying neutron production and the Bi was of sufficient thickness (2.5 cm) such that the Bi neutron resonances in the keV region were black; this enabled a constant monitoring of the low-energy background. The detector system at 36 m consisted of 1 kg of ^{10}B metal powder housed in a 12.5-cm-diam Al container which was viewed by 4 NaI detectors.[15]

The linac was operated at 720 pps with a 20-nsec-wide pulse and a peak current of ~0.5 A. The data-taking period per machine pulse was 100 μsec. The signals from the NaI detectors were transmitted to TOF hardware with an on-line computer sorting the information into histogram form.[17] The 4096 timing channels were divided into 4 groups, the first, second, third, and fourth group having 8-, 16-, 32-, and 64-nsec channel widths, respectively. This enabled data to be taken simultaneously over the energy range 1 keV to 1 MeV with good resolution.[18] Samples of interest were located 3 m from the neutron source and cycling of sample and open runs was carried out every 10 min.

The electron beam power was monitored by a $P2$ ionization chamber,[19] while the neutron beam intensity was recorded by a properly shielded BF_3 proportional counter. For the measurements presented here the beam normalization for sample and open runs implied by the $P2$ and BF_3 monitors agreed to within 0.5% or better. The background was found to have an energy-dependent and constant component. The constant background was cleanly identified with neutron-induced activity of the NaI crystals and was only important below several keV where the beam intensity was low; at 1 keV it contributed a 4% background. This constant background was easily subtracted out. The energy-dependent background at 250, 28, and 2 keV was determined by using filters of Li, Fe (not permanently in the beam), and Bi. At these energies this background was ~1%.

The excellent beam stability and background conditions of the National Bureau of Standards underground TOF system makes this facility ideally suited for very precise (< 1%) average transmission measurements. For reasons mentioned above this accuracy is essential for S_1 to be determined with good precision. As a test of the precision and reliability of the TOF system, a measurement of the carbon total cross section was made several times. Over the energy region of interest (≤600 keV) the carbon cross-section measurements made with this facility agreed with each other, to within statistics, and agreed to within 1 or 2% with other very precise measurements.[20]

SAMPLES

All samples used were at least 99% pure. Except for Rh and Ho, which had ~3.3-cm diameters, the standard format was 5.1-cm-diam samples. Nb, Rh, Ag, In, La, Ho, Au, and Th were self-supporting foils, whereas As, $AlBr_3$, Sb, and I were powders (≥ 100 mesh) pressed into containers. The open beam measurements for the elements in powder form had equivalent empty containers in the open beam. For $AlBr_3$, an appropriate amount of Al was placed in the open beam so that the experimentally measured transmission was that of Br only. Table I lists the sample thicknesses used.

ANALYSIS

After dead-time corrections were made the energy-independent background was subtracted. This left a residual 1% background which was not subtracted. With an average transmission ≳0.75 the 1% background enters in both sample and open runs, and consequently, has a negligible effect on the measured transmission. The data were processed into a T vs E format and then averaged over energy to form $\langle T\rangle_{exp}$. In the low-energy region 2-keV intervals were averaged increasing to 20 keV in the high-energy region. The next step in the analysis was to evaluate $\langle T\rangle$ theoretically for comparison with the data. The nature of the expression for $\langle T\rangle$ depends strongly on the sample thicknesses chosen. For example, if the samples are sufficiently thin, then $\langle e^{-n\sigma_T}\rangle \cong e^{-n\langle\sigma_T\rangle}$ and the theoretical average cross section is simply related to $\langle T\rangle_{exp}$ through:

$$\langle\sigma_T\rangle = -\frac{1}{n}\ln\langle T\rangle_{exp}. \qquad (2)$$

For the sample thicknesses employed in this experiment and, most importantly, considering the severe Doppler broadening of the $l=1$ resonances, the thin sample approximation was found to be valid for the p levels. This was examined analytically by estimating the self-protection of the p levels and comparing it with the thin sample-approximation result. Furthermore, an experimental test was made in the case of Nb, which has "strong" p levels, by running a thinner Nb sample ($1/n=55.7$). The value of S_1 (6.2×10^{-4}) found with the thinner sample was in good agreement with the "thick" Nb result (see Table II). The $l=0$ resonances are too strong at low energies for the thin sample approximation to be valid, except for undesirable thin samples where small uncertainties in the transmission imply large errors in $\langle\sigma_T\rangle$. Furthermore, it is important to analyze the data down to 1 keV so that a more accurate determination of R' (and hence $\sigma_{SE}^{l=0}$) can be made. Consequently, samples of intermediate thickness were used (see Table I) and the self-protection of the $l=0$ levels was accounted for where necessary.

Generally speaking, above 70 keV the thin sam-

TABLE I. Sample thicknesses of the elements and their s-wave parameters.

Element	Sample thickness $1/n$ (b/atom)	$10^4S_0\times10^4$	$\langle D\rangle$ (eV)	$\langle\Gamma_\gamma\rangle$ (meV)	Ref.
As	25.0	1.7	87.	300.	24
Br	29.9	1.2	36.	300.	24
Nb	24.9	0.36	90.	115.	25
Rh	73.4	0.54	27.	171.	26
Ag	26.3	0.48	10.6	136.	25,27
In	20.7	···	···	···	28
Sb	19.9	0.34	10.2	100.	29
I	30.4	0.64	14.3	110.	25
La	50.3	···	···	···	28
Ho	48.6	1.85	5.	75.	30
Au	35.3	1.9	16.2	125.	31
Th	32.6	0.86	16.8	21.2	32

ple approximation was valid. Therefore, a low-energy and a high-energy ($E > 70$ keV) expression for $\langle T \rangle$ was used in the analysis, but the data were fitted simultaneously over the whole energy range (1 keV $\leqslant E \leqslant$ 600 keV). The low-energy expression employed for $\langle T \rangle$ is:

$$\langle T \rangle = T_0 (1 - \langle A \rangle / \langle D \rangle) , \tag{3a}$$

$$\langle A \rangle = \int_0^\infty P(x) A(x,E) dx . \tag{3b}$$

$P(x)$ is the Porter-Thomas[21] distribution of the reduced neutron widths. $A(x, E)$ is the Doppler-broadened area resulting from a single level Breit-Wigner equation which includes self-interference and $\langle D \rangle$ is the average $l = 0$ spacing. The term $1-\langle A \rangle / \langle D \rangle$ represents the effect of the $l = 0$ levels. The remainder of the s-wave interaction and the total p-wave contribution to $\langle T \rangle$ are contained in T_0:

$$T_0 = \exp[-n\langle \sigma_T^{l=1} \rangle - n(\langle \sigma_T^{l=0} \rangle - \langle \sigma_R^{l=0} \rangle)] . \tag{3c}$$

The expressions employed for the total cross sections were obtained from the average R-matrix theory.[22] They are:

$$\langle \sigma_T^l \rangle = 2\pi \lambda\!\!\!^{-2} (2l+1)(1 - \mathrm{Re}\, \bar{U}_l) , \tag{4a}$$

and

$$\bar{U}_l = e^{-2i\phi_l} \left(\frac{1 - \bar{R}_l L_l^*}{1 - \bar{R}_l L_l} \right) , \tag{4b}$$

where

$$\phi_l = \tan^{-1}(-j_l / n_l) , \tag{4c}$$

$$\bar{R}_l = R_l^\infty + i\pi s_l , \tag{4d}$$

$$L_l = S_l + l + iP_l . \tag{4e}$$

The notation here is the same as that of Lane and Thomas[22] (S_l in the expression above is the shift function and not the strength function). The cross section for each partial wave is characterized by two unknown parameters, R_l^∞ and s_l. R_l^∞ represents the effects due to faraway levels and in the $l = 0$ case is related to R' at keV energies by the expression: $R' = R(1 - R_0^\infty)$. R is the nuclear radius which was taken to be $1.4 A^{1/3}$ fm. s_l is the *pole* strength function and is related to the strength function through:

$$S_l = \frac{2kRs_l}{(E/1\text{ eV})^{1/2}} . \tag{5}$$

In the expression for T_0,

$$\langle \sigma_R^{l=0} \rangle = 2\pi^2 \lambda\!\!\!^{-2} \left(\frac{E}{1\text{ eV}} \right)^{1/2} S_0 \cos(2\gamma_0), \tag{6a}$$

where

$$\gamma_0 = kR - \tan^{-1}(R_0^\infty kR). \tag{6b}$$

This term removes from $\langle \sigma_T^{l=0} \rangle$ the $l = 0$ contribution already accounted for by $(1 - \langle A \rangle / \langle D \rangle)$. At higher energies where the sample is becoming thin for $l = 0$ levels

$$e^{n\langle \sigma_R^{l=0} \rangle} (1 - \langle A \rangle / \langle D \rangle) \rightarrow 1 , \tag{7a}$$

and

$$\langle T \rangle \rightarrow \exp[-n(\langle \sigma_T^{l=1} \rangle + \langle \sigma_T^{l=0} \rangle)] . \tag{7b}$$

Also included in the expression for $\langle T \rangle$ was the d-wave contribution, expected to be small for $E < 600$ keV. Since the d- and s-wave parameters are expected to have similar behavior as a function of mass number it was assumed that $R_2^\infty = R_0^\infty$ and $s_2 = s_0$. Under these assumptions, the d-wave contribution to $\langle T \rangle$ was 1% or less *at 600 keV* for $75 \leqslant A \leqslant 139$ and a few % in the Ho, Au, and Th cases, diminishing rapidly with decreasing neutron energy. This method of analysis is similar to that used by others.[11,12,23]

The data were analyzed in the following way. The information necessary to calculate the $l = 0$ com-

TABLE II. Optimum parameters determined by fitting the data as described in the text.

Element	s_0	R_0^∞	R'	s_1	$10^4 S_1 \times 10^4$	R_1^∞
As	0.066	-0.145 ± 0.035	6.76 ± 0.25	0.105 ± 0.025	2.7 ± 0.6	-0.05 ± 0.1
Br	0.045	-0.14 ± 0.04	6.88 ± 0.35	0.145 ± 0.025	3.8 ± 0.6	0.2 ± 0.1
Nb	0.013	-0.07 ± 0.03	6.80 ± 0.25	0.215 ± 0.02	6.0 ± 0.6	0.2 ± 0.1
Rh	0.019	0.06 ± 0.05	6.2 ± 0.3	0.19 ± 0.03	5.5 ± 0.9	-0.1 ± 0.1
Ag	0.016	0.03 ± 0.03	6.46 ± 0.20	0.13 ± 0.02	3.8 ± 0.6	-0.15 ± 0.1
In	0.0087	0.095 ± 0.02	6.16 ± 0.16	0.105 ± 0.02	3.15 ± 0.6	-0.10 ± 0.1
Sb	0.011	0.09 ± 0.03	6.3 ± 0.2	0.070 ± 0.015	2.1 ± 0.5	-0.30 ± 0.1
I	0.021	0.145 ± 0.03	6.00 ± 0.25	0.050 ± 0.015	1.55 ± 0.5	-0.25 ± 0.1
La	0.022	0.27 ± 0.04	5.3 ± 0.3	0.016 ± 0.01	0.5 ± 0.4	-0.25 ± 0.1
Ho	0.055	0.01 ± 0.03	7.60 ± 0.25	0.02 ± 0.01	0.7 ± 0.4	-0.1 ± 0.1
Au	0.053	-0.14 ± 0.04	9.30 ± 0.35	0.012 ± 0.01	$0.4^{+0.4}_{-0.3}$	0.1 ± 0.1
Th	0.025	-0.13 ± 0.03	9.72 ± 0.30	0.04 ± 0.01	1.5 ± 0.4	0.1 ± 0.1

pound-nucleus contribution to $\langle T\rangle$, i.e., $(1-\langle A\rangle/\langle D\rangle)$, was obtained from *previously published* data.[24-32] Specifically, S_0, $\langle D\rangle$, and $\langle\Gamma_\gamma\rangle$ (average s-wave radiation width) were obtained from low-energy high-resolution data. The values used are listed in Table I. This reduces the number of unknowns to three, R_0^∞, s_1, and R_1^∞. Although the whole energy region (1 keV $\leq E \leq$ 600 keV) was used to determine the unknowns, certain energy regions are more sensitive to one parameter than another. Below 100 keV the influence of R_1^∞ ($l=1$ shape elastic scattering) is effectively zero. s_1 is determined mainly by the data in the energy region $30 < E < 200$ keV,[33] and even though R_0^∞ has a large effect on $\langle T\rangle$ at all energies measured, the data below ~30 keV go far toward determining R_0^∞. Consequently, although there are three unknowns the fitting at a given energy usually involves only two parameters.

In order to determine what constitutes the best fit of the theoretical transmission to the experimental transmission, the sum $x=\sum_J[\langle T\rangle_{\text{exp}}^J-\langle T\rangle^J]^2$ was evaluated for each trial set of parameters. The sum x had a well defined minimum and this determined the selected values of R_0^∞, s_1, and R_1^∞. The curves representing the best fits are shown in Fig. 2. The dashed curves represent the s-wave contribution to $\langle T\rangle$ while the solid curves give the theoretical transmission with the chosen s- and p-wave parameters which are listed in Table II. As the parameters were changed from their optimum values the value of x increased and the fits to the data became less satisfactory. The quoted uncertainties of R_0^∞, s_1, and R_1^∞ were determined by the range of values which gave acceptable fits. An example of an unacceptable fit is shown for the case of Ag, see Fig. 2. The solid curve which fits the data well was calculated with the parameters given in Table II. The short dashed curve was calculated with $R_0^\infty=0.01$, $s_1=0.10$, and $R_1^\infty=0.30$. The values of s_1, R_1^∞ are barely outside the quoted uncertainties, but the fit to the data is clearly unacceptable.

The statistical precision of the data points in Fig. 2 is better than 1%. Therefore, much of the scatter in the value of $\langle T\rangle$ at low energies can be attributed to the fluctuations of the finite number of resonances in an energy interval. For example, the Nb levels have $\langle D\rangle^{l=0}=90$ eV while In has $\langle D\rangle^{l=0}=5$ eV. As expected, the In data are much smoother. The behavior of $\langle T\rangle$ vs energy is rather "flat" in general. The $l=0$ contribution to $\langle T\rangle$ decreases slowly with increasing energy while the $l=1$ contribution slowly increases. In the case of In these opposing effects result in a flat transmission. For the case of Au the s interaction dominates and the transmission increases with increasing energy. The opposite situation exists for Nb where the p interaction is very strong.

In this analysis R_0^∞, s_1, and R_1^∞ are treated as being energy-independent. The optical model indicates, however, that these parameters are energy-dependent. However, as discussed above, except for R_0^∞, they have an important influence on the

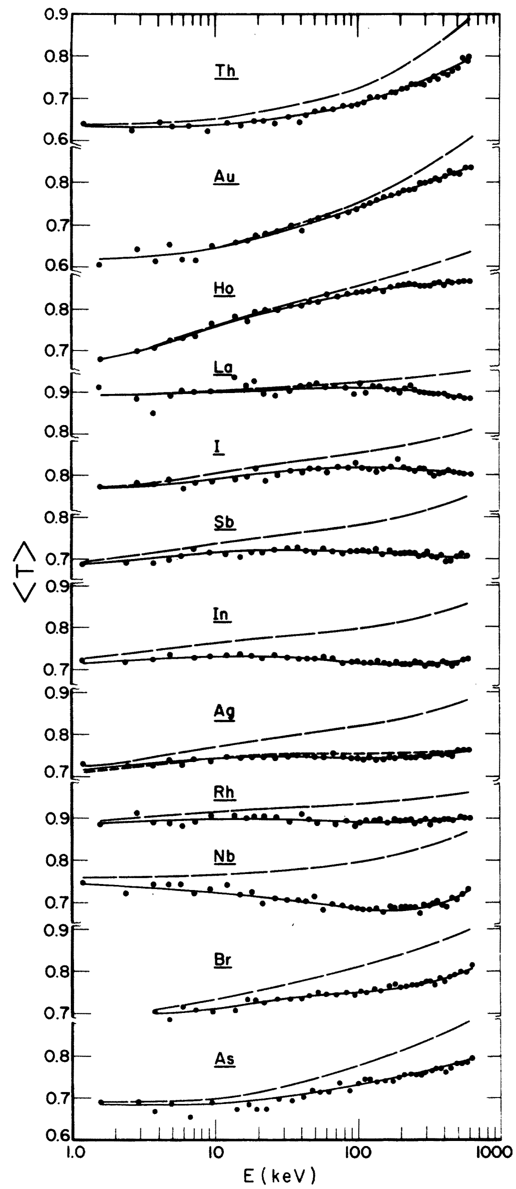

FIG. 2. The average transmission vs neutron energy. The points represent the experimental data and have a statistical accuracy of better than 1%. The long dashed curve gives the calculated $l=0$ average transmission using the optimum parameters, while the solid curve represents the calculated average transmission with s-, p-, and d-wave contributions as described in the text. For Ag the short dashed curve is an example of an unacceptable fit to the data.

transmission only over limited energy regions and any inherent energy variation should not be significant. As a *guide* to the possible energy dependence of R_0^∞ the following calculation was performed. Using Moldauer's optical potential[34] (see below) $\sigma_{SE}^{l=0}$ and $\sigma_C^{l=0}$ were calculated at $E = 1$ keV. Equating these cross sections to the corresponding R-matrix expressions:

$$\langle\sigma_{SE}^{l=0}\rangle = \pi\lambda\!\!\!^{-2}\,|1-\bar{U}_0|^2\,, \tag{8a}$$

$$\langle\sigma_C^{l=0}\rangle = \pi\lambda\!\!\!^{-2}\,(1-|\bar{U}_0|^2)\,, \tag{8b}$$

values of R_0^∞ and s_0 were found. $\sigma_{SE}^{l=0}$ was then calculated over the energy range 1 to 600 keV using the optical model and the R-matrix expressions. Any deviation of $\sigma_{SE}^{OP}/\sigma_{SE}^{RM}$ from unity was taken as evidence that R_0^∞ was varying with energy. In the mass region $75 \leq A \leq 139$ the determination of S_1 is unaffected by the slight energy dependence of R_0^∞. However, in other mass regions where S_0 and R' are large *and* S_1 is small this can be important. For example, Au, with $S_0 = 1.9\times10^{-4}$, lies close to the 4S $l=0$ strength-function maximum and has a large shape elastic cross section (R' = 9.3 fm, see Table II). In addition, the p-wave strength function appears to be very small. In this case the small deviation (~4%) of $\sigma_{SE}^{OP}/\sigma_{SE}^{RM}$ from unity has a significant effect on the implied value of S_1. For these reasons the quoted uncertainty of the p-wave strength function for Au and, to a lesser extent, Ho, is larger than implied by the fitting procedure as described above.

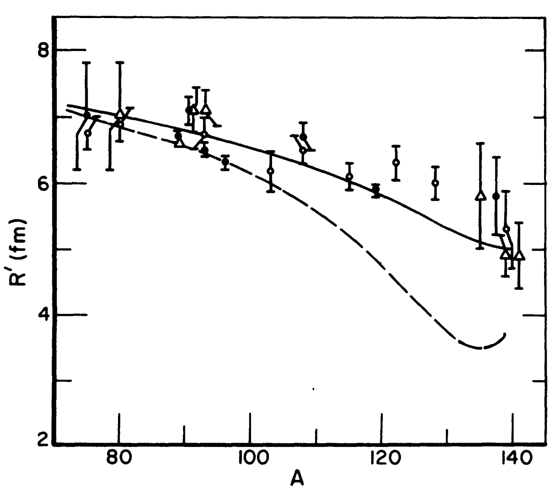

FIG. 3. The $l = 0$ elastic scattering length R' vs mass number A. ● represents results from Ref. 35, △ from Ref. 36, and ○ results of this experiment. The solid curve was calculated using Moldauer's optical potential. The dashed curve was calculated with the same form of the potential but with the constants altered to fit the p-wave data.

RESULTS

The quantities of interest here are R_0^∞ (and hence R') and S_1. Values of R' determined previously[35,36] are plotted in Fig. 3 along with values found here [determined by the relationship $R' = R(1-R_0^\infty)$ mentioned previously] for the region $75 \leq A \leq 139$. As is evident from Fig. 3, the agreement with previous results is good where there is overlap or where they otherwise follow the trend indicated by neighboring values. Figure 4 shows the value of the p-wave strength function S_1 determined here for $75 \leq A \leq 139$. Some previous measurements[11,36,37] of S_1 are also included in Fig. 4 and were determined using methods (1) or (3) as described in the Introduction. It is worth noting that the S_1 values determined in this experiment are representative of the p-wave interaction at ~100 keV. Other S_1 values plotted in Fig. 4 (△, □) are representative of the p-wave interaction below ~15 keV. However, since the change of S_1 with energy over a 100-keV interval is expected to be small (and well within the quoted uncertainties), it is meaningful to

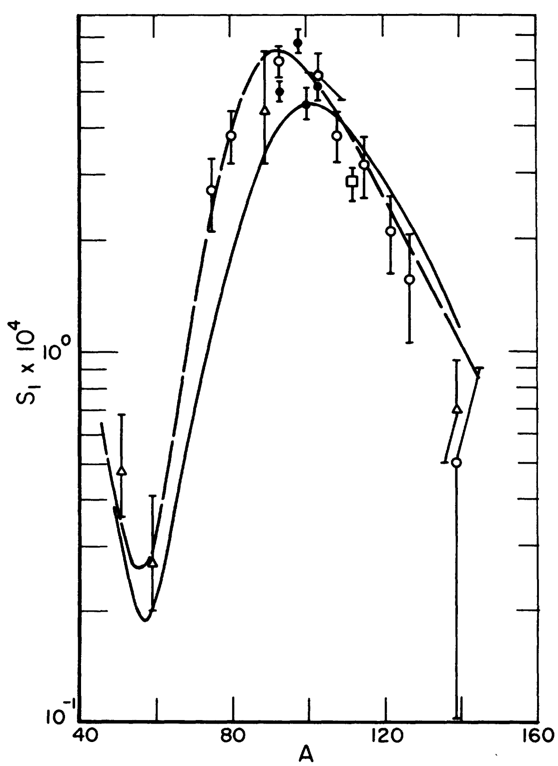

FIG. 4. The p-wave strength function S_1 vs mass number A. ● represents results from Ref. 11, △ from Ref. 36, □ from Ref. 37, and ○ results of this experiment. The dashed and solid curves were generated as described for Fig. 3.

plot these data together.

As can be seen from Fig. 4, the agreement among the measurements is quite satisfactory. In addition (see Table II), the value of $S_1 = 0.7 \pm 0.4 \times 10^{-4}$ obtained for Ho agrees well with that obtained by Liou *et al.*[7] ($S_1 = 0.7 \pm 0.2 \times 10^{-4}$) for ^{168}Er, a neighboring nucleus. Furthermore, the value of $S_1 = 1.5 \pm 0.4 \times 10^{-4}$ found for Th is in good agreement with the Harwell[11] result ($S_1 = 1.65 \pm 0.20 \times 10^{-4}$).

Figure 4 shows a strong peaking of S_1 near $A = 100$ and also *no* indication of any "splitting" of the maximum as a consequence of the spin-orbit interaction. The optical-model calculations performed here and elsewhere[34] indicate that the p-wave strength function,

$$S_1 = \frac{1}{3}\frac{\langle g\Gamma_n^1\rangle}{\langle D\rangle} = \frac{1}{3}\left[g_+ \frac{\langle\Gamma_n^1\rangle^+}{\langle D\rangle^+} + g_- \frac{\langle\Gamma_n^1\rangle^-}{\langle D\rangle^-}\right], \tag{9}$$

is insensitive to the spin-orbit potential even though $\langle\Gamma_n^1\rangle^+/\langle D\rangle^+$ and $\langle\Gamma_n^1\rangle^-/\langle D\rangle^-$ can be very sensitive (+ and − meaning $l+\frac{1}{2}$, $l-\frac{1}{2}$, respectively). For example, on the sides of the maximum, $A = 80$, 115, $\langle\Gamma_n^1\rangle^+/\langle D\rangle^+$ and $\langle\Gamma_n^1\rangle^-/\langle D\rangle^-$ can easily differ by a factor of 2. (In fact, a good place to look for a difference between the + and − strength functions is on the sides of the maximum and not at the peak where their values can be quite similar.) Since the average transmission measurement is sensitive to S_1, no effect of the spin-orbit term is observed.

The strength function S_1 is sensitive to how an $l = 1$ neutron "sees" the nucleus. In order to test for any possible difference between $l = 0$ and $l = 1$ potentials it is necessary to have an optical potential which gives a good fit to the $l = 0$ data. Of the efforts in this direction,[34,38,39] Moldauer's work seems best—at least for nuclei where the spherical potential is applicable. He obtained good fits to the s-wave strength-function data and R' for the mass region $40 \leq A \leq 140$. Moldauer's form of the potential and final choice of constants are:

$$V = -V_0 q(r) - iWp(r) + V_{so}\left[\frac{\hbar}{M_\pi C}\right]^2 \vec{\sigma}\cdot\vec{1}\frac{1}{r}\frac{d}{dr}q(r), \tag{10a}$$

$$q(r) = \left[1 + \exp\left(\frac{r-R}{a}\right)\right]^{-1}, \tag{10b}$$

$$P(r) = \exp - \left(\frac{(r-R-d)}{b}\right)^2, \tag{10c}$$

where

$$\begin{aligned} &V_0 = 46, \quad R = 1.16A^{1/3} + 0.6,\\ &W = 14, \quad a = 0.62,\\ &V_{so} = 7, \quad b = 0.50,\\ &\qquad\qquad d = 0.50. \end{aligned} \tag{10d}$$

All potential strengths are in MeV and lengths are in fermis. With $d = 0.0$ the imaginary part of the potential would peak at the nuclear radius. A value of $d = 0.5$ causes the absorptive potential to peak outside the nuclear radius. This is consistent with theoretical studies[40] and was introduced in order to reproduce the observed minimum of S_0 at $A = 100$.

Using this potential, R' and S_1 were calculated as a function of A at $E = 1$ keV. For example, in order to calculate S_1, $\sigma_C^{l=1}$ was calculated at 1 keV and equated to:

$$6\pi^2\lambda\!\!\!^{-2}\left(\frac{E}{1\ \text{eV}}\right)^{1/2}\frac{(kR)^2}{1+(kR)^2}S_1\,. \tag{11}$$

With $R = 1.4A^{1/3}$ fm a value of S_1 was determined. The solid curves of Figs. 3 and 4 represent the results. The agreement between the predicted and experimental values of S_1 is poor. The data indicate a stronger peaking of S_1 (implying a *weaker* imaginary potential strength or a more diffuse potential) at a lower mass number. This latter feature of the data implies that an $l = 1$ neutron experiences a stronger real potential strength than an $l = 0$ neutron. If the constants of the potential are changed slightly, $V_0 \to 47$ and $a \to 0.72$, the result is the dashed curves of Figs. 3 and 4. While Fig. 4 shows the dashed curve agreeing well with

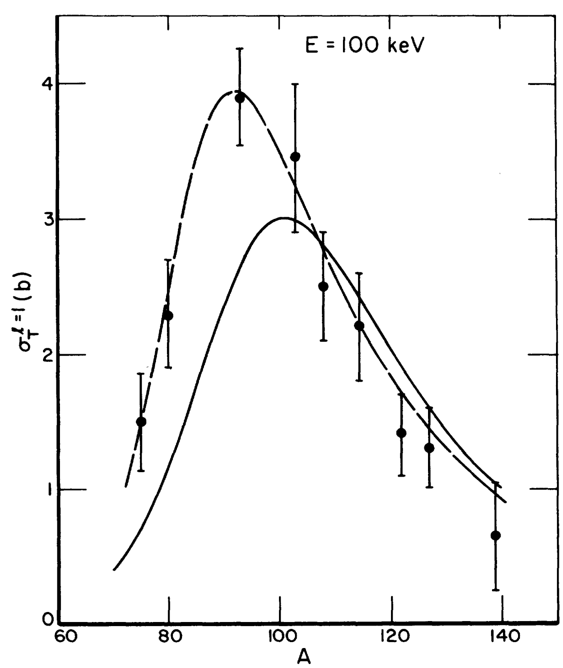

FIG. 5. The p-wave total cross section vs mass number A at the energy $E = 100$ keV. The "data" points were calculated using the optimum p-wave parameters determined in this experiment. The dashed and solid curves were generated as described for Fig. 3.

the p-wave data, Fig. 3 shows a poor fit to the $l=0$ R' data. The implication is that when the potential is made to fit the p-wave data, the fit to the $l=0$ data becomes unacceptable and vice versa.[41] This suggests that an $l=0$ and $l=1$ neutron experience different potentials. The same conclusions are reached if the p-wave total cross section is examined at higher energies. Figure 5 shows the total $l=1$ cross section vs mass number at $E=100$ keV. The "data" points were calculated using the optimum p-wave parameters determined in this experiment. The solid and dashed curves were calculated with the potential parameters as described above, and again one sees that the potential as determined by the $l=0$ data does not give satisfactory fits to the p-wave data.

The p-wave data indicate that an $l=1$ neutron experiences a stronger real potential than an $l=0$ neutron. In this connection it is worth noting a calculation by Lemmer[42] of the *bound*-state problem using a nonlocal potential in the effective mass approximation. He was led to the usual Schrödinger equation, but with an effective mass, and with additional terms resulting from the nonlocality of the potential. Some of the additional terms were a function of the orbital angular momentum of the nucleon, and for a spherically symmetric potential a $-C^2\vec{l}\cdot\vec{l}$ term can easily be identified. This term results in a stronger potential for nucleons with higher orbital angular momentum. To the extent that the real part of the *low-energy* optical potential is similar to the potential a bound-state nucleon experiences, these terms might arise also.

SUMMARY

Precise average neutron-transmission measurements were performed for 12 elements and R' and S_1 were extracted from the data. The values of R' found here agree well with previous values where there is overlap. The S_1 values found are in good agreement with other accurate measurements and are sufficiently precise to give a picture of the behavior of S_1 in the mass region $A=100$. The optical-model calculations indicate that the $l=0$ and $l=1$ data cannot be fitted simultaneously using a potential with the same constants. This implies an orbital angular momentum dependence of the low-energy optical potential.

ACKNOWLEDGMENTS

It is my pleasure to acknowledge the constant support and encouragement of Dr. R. B. Schwartz throughout all phases of this research as well as useful discussions. I wish to express my gratitude to R. A. Schrack and especially to H. T. Heaton, II, and J. Menke for help with the measurements and for many discussions which enabled me to better understand the experimental setup. My thanks to H. I. Liou for helpful suggestions.

Of considerable help were the samples provided me by Professor J. Rainwater and Dr. C. D. Bowman. Lastly, I thank the linac operators for their extra effort in providing a stable electron beam.

---

*National Research Council-National Bureau of Standards (U. S.) postdoctoral research associate, 1972–1973.

[1] H. Feshbach and V. F. Weisskopf, Phys. Rev. 76, 1550 (1949).

[2] H. H. Barschall, Phys. Rev. 86, 431 (1952); D. W. Miller, R. K. Adair, C. K. Bockleman, and S. E. Darden, Phys. Rev. 88, 83 (1952).

[3] H. Feshbach, C. Porter, and V. F. Weisskopf, Phys. Rev. 96, 448 (1954).

[4] For $E<100$ keV $\sigma_T^{l=1} \cong 6\pi^2 ƛ^2 (E/1\text{ eV})^{1/2}\{(kR)^2/[1+(kR)^2]\} \times S_1$, where S_1 is the p-wave strength function defined in the text. At higher energies the $l=1$ shape elastic scattering becomes important as do higher-order terms in S_1.

[5] A. Saplakoglu, L. M. Bollinger, and R. E. Cote, Phys. Rev. 109, 1258 (1958).

[6] H. I. Liou, H. S. Camarda, and F. Rahn, Phys. Rev. C 2, 1002 (1972).

[7] H. I. Liou, H. S. Camarda, S. Wynchank, M. Slagowitz, G. Hacken, F. Rahn, and J. Rainwater, Phys. Rev. C 5, 974 (1972).

[8] S. F. Mughabghab, in Proceedings of the Third Conference on Neutron Cross Sections and Technology, Knoxville, 1971 (unpublished).

[9] J. H. Gibbons, R. L. Macklin, P. D. Miller, and J. H. Neiler, Phys. Rev. 122, 989 (1961).

[10] D. Kompe, Nucl. Phys. A133, 513 (1969).

[11] C. A. Uttley, C. M. Newstead, and K. M. Diment, in *Proceedings of the Conference on Nuclear Data for Reactors, Paris, 1966* (International Atomic Energy Agency, Vienna, 1967), Vol. I, p. 165.

[12] A. P. Jain, R. E. Chrien, J. A. Moore, and H. Palevsky, Phys. Rev. 137, B83 (1965).

[13] K. K. Seth, R. H. Tabony, E. G. Bilpuch, and H. W. Newson, Phys. Lett. 13, 70 (1964).

[14] M. Divadeenam *et al.*, private communication (to be published).

[15] H. T. Heaton, II, R. B. Schwartz, and R. A. Schrack, Bull. Am. Phys. Soc. 17, 461 (1972); J. L. Menke and R. A. Schrack, *ibid.*, p. 894.

[16] H. S. Camarda, Nucl. Instrum. Methods 106, 205 (1973).

[17] H. T. Heaton, II, Natl. Bur. Std. (U. S.) Technical Note No. 515, 1970 (unpublished).

[18] Although the interest here is a "poor" resolution experiment, the good resolution was vital for determining

the background conditions.

[19]J. S. Pruitt and S. R. Domen, Natl. Bur. Std. (U. S.) Monograph No. 48, June 1952 (unpublished).

[20]C. A. Uttley and K. M. Diment, in Proceedings of the Symposium on Neutron Standards and Flux Normalization, Argonne, Illinois, 1971 (unpublished), p. 201; R. B. Schwartz, H. T. Heaton, II, and R. A. Schrack, *ibid.*, p. 377.

[21]C. E. Porter and R. G. Thomas, Phys. Rev. 104, 483 (1956).

[22]R. G. Thomas, Phys. Rev. 97, 224 (1955); A. M. Lane and R. G. Thomas, Rev. Mod. Phys. 30, 257 (1958); P. A. Moldauer, Phys. Rev. 129, 754 (1963); E. W. Vogt, Rev. Mod. Phys. 34, 723 (1962).

[23]J. E. Lynn, Proc. Phys. Soc. Lond., 82, 903 (1963).

[24]J. Julian, G. Bianchi, C. Gorge, V. D. Huynh, G. Le Poittevin, J. Morgenstern, F. Netter, and C. Samour, Phys. Lett. 10, 86 (1964); J. B. Garg, W. W. Havens, Jr., and J. Rainwater, Phys. Rev. 136, B177 (1964).

[25]J. B. Garg, J. Rainwater, and W. W. Havens, Jr., Phys. Rev. 137, B547 (1965).

[26]P. Ribon, J. Girard, and J. Trochon, Nucl. Phys. A143, 130 (1970).

[27]R. E. Chrien, Phys. Rev. 141, 1129 (1966).

[28]G. Hacken, Ph.D. thesis, Columbia University, 1971 (unpublished).

[29]S. Wynchank, J. G. Garg, W. W. Havens, Jr., and J. Rainwater, Phys. Rev. 166, 1234 (1968).

[30]M. Asghar, C. M. Chaffey, and M. C. Moxon, Nucl. Phys. A108, 535 (1968); E. N. Karzhavina, A. B. Popov, Yu. S. Yazvitskie, V. N. Efimov, and N. Yu. Shirikova, Yad. Fiz. 5, 471 (1967) [transl.: Sov. J. Nucl. Phys. 5, 329 (1967)]; H. Tellier and C. M. Newstead, in Proceedings of the Third Conference on Neutron Cross Sections and Technology, Knoxville, 1971 (unpublished).

[31]R. N. Alves, J. Julien, J. Morgenstern, and C. Samour, Nucl. Phys. A131, 450 (1969).

[32]P. Ribon, Ph.D. thesis, Université de Paris, 1969 (unpublished); F. Rahn, H. S. Camarda, G. Hacken, W. W. Havens, Jr., H. I. Liou, J. Rainwater, M. Slagowitz, and S. Wynchank, Phys. Rev. C 6, 251 (1972).

[33]$\sigma_C^{l=1}$ starts to decrease above 200 keV while the $l=1$ shape elastic cross section increases.

[34]P. A. Moldauer, Nucl. Phys. 47, 65 (1963).

[35]K. K. Seth, D. J. Hughes, R. L. Zimmerman, and R. C. Garth, Phys. Rev. 110, 692 (1958).

[36]J. Morgenstern, R. N. Alves, J. Julien, and C. Samour, Nucl. Phys. A123, 561 (1969).

[37]H. I. Liou *et al.*, private communication.

[38]B. Buck and F. G. Perey, Phys. Rev. Lett. 8, 444 (1962).

[39]A. P. Jain, Nucl. Phys. 50, 157 (1963).

[40]L. C. Gomes, Phys. Rev. 116, 1226 (1959).

[41]If the following changes of the constants of the potential are made, $V_0 \rightarrow 47.1$, $W \rightarrow 12.$, $a \rightarrow 0.68$, a good fit to the *p*-wave data is obtained. However, the fit to the $l=0$ data is again rather poor.

[42]R. H. Lemmer, Phys. Rev. 117, 1551 (1960).